Signal Processing 219 (2024) 109427

Contents lists available at ScienceDirect

Signal Processing

journal homepage: www.elsevier.com/locate/sigpro

# Bi-orthogonality recovery and MIMO transmission for FBMC systems based on non-sinusoidal orthogonal transformation

Ying Wang [a,b], Qiang Guo [a,b], Jianhong Xiang [a,b,*], Linyu Wang [a,b], Yang Liu [c]

[a] College of Information and Communication Engineering, Harbin Engineering University, Harbin 150001, China
[b] Key Laboratory of Advanced Ship Communication and Information Technology, Harbin Engineering University, Harbin 150001, China
[c] Agile and Intelligent Computing Key Laboratory, China Electronic Technology Group(cetc-10), Chengdu 610036, China

ARTICLE INFO

*Keywords:*
Bi-orthogonal FBMC
Offset-QAM
MIMO
Walsh transform
Bi-orthogonality recovery

ABSTRACT

Filter Bank Multi-Carrier (FBMC) system based on offset Quadrature Amplitude Modulation (offset-QAM) combined with Multiple-Input-Multiple-Output (MIMO) technique faces great challenges. The inherent imaginary interference of FBMC seriously impacts the performance of the Maximum Likelihood (ML) detection technique in MIMO transmission. The application of the Alamouti code is also hindered. In this paper, we present a data-compressed transmission method based on non-sinusoidal orthogonal transformation, which can recover the bi-orthogonality of FBMC and eliminate the imaginary interference. Thereby, the combination of FBMC and MIMO as well as the application of ML technique and Alamouti code are realized. Specifically, we first consider the Walsh transform, which belongs to the non-sinusoidal orthogonal transform, and utilize its property that can reduce the transmission bandwidth to recover the orthogonality of the FBMC in the frequency domain. Secondly, we construct the discrete transmission model of the system and generate the orthogonal compression matrix utilizing the fast Walsh transform. Then, we analyze the multi-frame transmission, calculate the frames interference, and improve the signal-to-interference ratio again by adding guard time slots. Finally, we construct the MIMO transmission model and complete the theoretical analysis. Simulation results show that the proposed scheme has a robust MIMO transmission performance. ML and Alamouti code techniques perform the same as Orthogonal Frequency Division Multiplex in bi-orthogonal FBMC.

## 1. Introduction

Future wireless networks should support multiple use case sharing, including massive Machine-Type Communication (mMTC) and Non-Terrestrial Networks (NTN) in 5G ecosystems [1,2]. The Orthogonal Frequency Division Multiplex (OFDM) used in 5G New Radio (NR) requires a license-based synchronization process to guarantee the orthogonality of the subcarriers. Additionally, the poor spectral properties of conventional OFDM lead to high sensitivity to timing errors. Although OFDM with filtering can improve the spectral properties [3], its out-of-band emission remains higher than that of FBMC [4]. In particular, OFDM and MIMO-OFDM have a large scope of parallel processing [5–7]. However, this requires precise time positioning and carrier synchronization. Relying on good time–frequency properties of the prototype filter, Filter Bank Multi-Carrier (FBMC) system based on offset Quadrature Amplitude Modulation (offset-QAM) gets rid of strict synchronization and is suitable for asynchronous transmission [8–11]. Therefore, FBMC supports asynchronous user coexistence, see Fig. 1. Although the Third Generation Partnership Project (3GPP) did not select FBMC as the 5G waveform, the technology is still a significant choice for future wireless system development [12]. Examples include carrier aggregation, cognitive radio, and Dense Wavelength Division Multiplex-based Passive Optical Networks (DWDM-PON) [13–15] etc. Now, FBMC has been included as priority research in EU projects such as 5GNOW and PHYDYAS [16,17].

However, FBMC based on offset-QAM (referred to as FBMC) ensures no loss of spectral efficiency by compressing the time-frequency spacing, which results in FBMC failing to guarantee complex orthogonality (i.e., bi-orthogonality). Therefore, the system suffers from inherent imaginary interference. Generally, this inherent interference carries very little information and is not worth detecting for reconstruction [18]. Moreover, this inherent interference significantly limits the application of Maximum Likelihood (ML) detection technique and Alamouti space–time block code in Multiple-Input Multiple-Output (MIMO) [19]. To combine MIMO with FBMC, a Fast Fourier Transform

* Corresponding author at: College of Information and Communication Engineering, Harbin Engineering University, Harbin 150001, China.
*E-mail addresses:* wangyingstu@163.com (Y. Wang), guoqiang@hrbeu.edu.cn (Q. Guo), xiangjianhong@hrbeu.edu.cn (J. Xiang), wanglinyu@hrbeu.edu.cn (L. Wang).

https://doi.org/10.1016/j.sigpro.2024.109427
Received 3 August 2023; Received in revised form 2 February 2024; Accepted 10 February 2024
Available online 12 February 2024

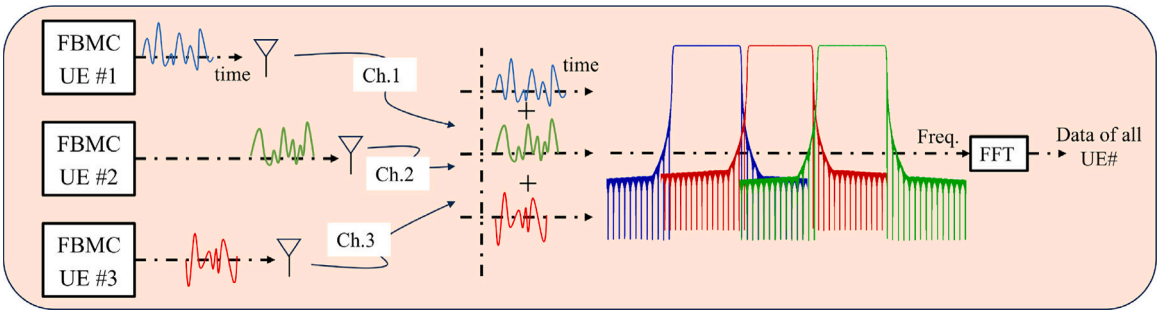


**Fig. 1.** FBMC asynchronous transmission with three asynchronous users coexisting. In fact, FBMC supports the coexistence of more asynchronous users.

(FFT) extension scheme was proposed in [20]. The scheme extends the transmitted symbols into the time (or frequency) domain, thus achieving interference cancellation. However, the FFT is a complex type of sinusoidal orthogonal transform. Consequently, the scheme has residuals of interference when performing symbol extension. Also, the complexity becomes higher because of the extra FFT operations. An improved Orthogonal Approximate Message Passing (OAMP) algorithm was proposed in [21] to achieve the optimal mean square error estimation. However, OAMP's matrix inversion for each iteration leads to high computational complexity. Chrislin Lélé et al. [22] adopted the Hadamard matrix to extend the transmitted symbols to the time domain and realized the combination of FBMC and Alamouti space–time block code. However, some possible interferences are not considered, e.g., interferences between data frames during multi-frame transmission. Ronald Nissel et al. [23] similarly employed Hadamard matrix to extend the symbols to the time domain and verifies the feasibility of MIMO. However, it lacks MIMO theoretical modeling, and the underlying structure of MIMO transmission is not sufficiently clear. On the other hand, to realize the compatibility between FBMC and OFDM, we need to consider various factors, including bi-orthogonality, frame interference and data transmission rate, etc. Unlike [23], our approach mainly relies on the column rate returned by the Walsh function to achieve signal compression and evaluation. The main contributions of this paper are summarized as follows:

- We present a bi-orthogonality recovery method based on non-sinusoidal orthogonal transformation. The Walsh transform is a non-sinusoidal orthogonal transform based on binary sequences. It can reduce the redundancy of the signal and compress the data in the frequency domain. We utilize its capability to compress signals and reduce the data transmission bandwidth. Thereby, the orthogonality of FBMC in the frequency domain is recovered.
- We derive Signal-to-Interference Ratio (SIR) closure expressions for adjacent data frames. Because the generation of the compression matrix strictly depends on the subcarrier numbers and the symbol numbers, the system can only compress the data symbols frame-by-frame. It leads to the bi-orthogonal FBMC's orthogonality only holds in the current data frame. At data frame boundaries, the transmission power exists in an excess zone and thus frame interference exists.
- We reduce the complexity of combining FBMC with MIMO. The bi-orthogonal FBMC has nearly the same orthogonal performance as OFDM, and the inherent imaginary interference is significantly mitigated. Therefore, when combined with the MIMO technique, bi-orthogonal FBMC has the same complexity as OFDM.
- We prove that the bi-orthogonal FBMC is compatible with CP-OFDM at many levels. For example, bi-orthogonal FBMC has the same information rate as OFDM, ML technique and Alamouti space–time block code have the same performance in bi-orthogonal FBMC as CP-OFDM, etc.

Notations: Bold capital letters and lowercase letters denote matrices and vectors, respectively. $\mathrm{diag}\{\cdot\}$ denotes the diagonal elements of a matrix. $\mathrm{vec}\{\cdot\}$ denotes vectorized operation by column. $\mathrm{E}\{\cdot\}$ denotes expectation. $\Re\{\cdot\}$ and $\Im\{\cdot\}$ denote the extract real and imaginary part operations, respectively. $(\cdot)^*$, $(\cdot)^T$ and $(\cdot)^H$ denote the complex conjugate, transposition, and conjugate (Hermitian) transposition, respectively. $\otimes$ denotes the Kronecker product. $\mathbf{I}_n$ denotes the $n \times n$ unit matrix. The imaginary unit is denoted as $\mathrm{j} = \sqrt{-1}$. $\mathbb{R}$ denotes the real domain and $\mathbb{C}$ the complex domain. $\mathbb{N}+$ denotes the positive integer.

## 2. System model

In FBMC, we modulate the data symbol $x_{l,k}$ utilizing the transmitted base pulse $g_{l,k}(t)$ [24]. If the transmitted signal $s(t)$ consists of $L$ subcarriers and $K$ time symbols, then we can express it as

$$s(t) = \sum_{l=1}^{L}\sum_{k=1}^{K} x_{l,k} \underbrace{p_{TX}(t-kT)\mathrm{e}^{\mathrm{j}2\pi lF(t-kT)}\mathrm{e}^{\mathrm{j}\frac{\pi}{2}(l+k)}}_{g_{l,k}(t)}. \tag{1}$$

Where $l$ denotes the frequency position and $k$ the time position. $F$ denotes the frequency spacing and $T$ the time spacing. $p_{TX}(t)$ denotes the transmitted prototype filter. This paper adopts the PHYDYAS prototype filter [25]. The received signal $r(t)$ can be obtained by passing $s(t)$ through the wireless channel, which can be expressed as

$$r(t) = \int_{\mathbb{R}} s(\tau)h(t-\tau)d\tau + \mathrm{n}(t). \tag{2}$$

Where $h(t)$ denotes the channel impulse response and $\mathrm{n}(t)$ the Additive Gaussian white noise. At the receiver (with the same prototype filter as the transmitter), projecting $r(t)$ to the received base pulse, we can obtain the received symbol $y_{l,k}$.

$$y_{l,k} = \int_{\mathbb{R}} r(t)g^*_{l,k}(t)dt. \tag{3}$$

Over the AGWN channel, employing matched filtering maximizes the Signal-to-Noise Ratio (SNR) and enables symbol recovery to be performed without inter-symbol interference [26].

In OFDM, $p_{TX}(t)$ is a rectangular function and the received prototype filter $p_{RX}(t)$ is a rectangular function with CP removed. Therefore, the base pulses are orthogonal, that is

$$\langle g_{l_1,k_1}(t), g_{l_2,k_2}(t)\rangle = \int_{\mathbb{R}} g_{l_1,k_1}(t)g^*_{l_2,k_2}(t)dt = \delta_{D_l,D_k}. \tag{4}$$

Where $\delta$ is the Kronecker function, $D_l = l_1 - l_2$, $D_k = k_1 - k_2$. However, in FBMC, the offset-QAM based transmission scheme compresses the time-frequency spacing to improve the spectral efficiency [4]. Thus, orthogonality holds only in the real domain, i.e., $\Re\{\langle g_{l_1,k_1}(t), g_{l_2,k_2}(t)\rangle\} = \delta_{D_l,D_k}$. The major problem with this FBMC transmission scheme is the imaginary interference, and only real value data symbols can be transmitted. Due to imaginary interference, ML detection must calculate a large number of possibilities, which makes ML detection techniques unable to be applied to traditional FBMC directly [23]. On the other hand, many techniques of OFDM systems cannot be directly applied to FBMC [23]. Examples include Alamouti space–time block code, etc. In a Single-Input Single-Output (SISO) system, we can eliminate

imaginary interference by real extraction. However, more compatibility issues between FBMC and OFDM cannot be resolved [27]. The aim of our work is to recover the biorthogonality of FBMC and achieve the preliminary compatibility between FBMC and OFDM.

## 3. Bi-orthogonal FBMC

Balian-Low theorem [28] indicates that a multi-carrier system cannot satisfy the bi-orthogonality, maximum spectral efficiency, time localization and frequency localization simultaneously. For example, OFDM sacrifices frequency localization and FBMC sacrifices biorthogonality. If the transmitted data symbols can be represented as a sum of square waves with different frequencies in the frequency domain, then the transmission bandwidth can be reduced [29]. Further, the biorthogonality of FBMC can be expected to be recovered in the frequency domain. Unfortunately, this comes at the cost of time-localization. Restoring biorthogonality in the frequency domain requires an improvement in frequency localization. Thus, according to Heisenberg's principle, no matter how hard we try to retain the FBMC performance, the time localization will deteriorate. Accordingly, some important implications need to be considered, see Section 3.3.

### 3.1. Symbol compression

In FBMC, the $L\times K$ time-frequency 2-D plane can transmit complex symbols as $\tilde{x}_{l,\kappa}$, where $\kappa \in [1,\dots K/2\,]$. For the $l$th symbol with length $K/2$ , we adopt the Walsh transform [30] for compression, which can be expressed as

$$\begin{aligned} x_{l,k} &= \frac{1}{\sqrt{K}}\sum_{\kappa=1}^{K/2}\tilde{x}_{l,\kappa}\omega(\kappa,k) \\ st.\quad \omega(\kappa,k) &= (-1)^{\sum_{i=1}^{\log_2(K/2)}\left\lfloor\frac{2\kappa-1}{2^i}\right\rfloor\left\lfloor\frac{k}{2^i}\right\rfloor}. \end{aligned} \tag{5}$$

Where $k \in [1,\dots,K]$, $\lfloor\cdot\rfloor$ denotes the downward rounding operation. Note that the compressed symbol $x_{l,k}$ is still complex-valued. At the receiver, performing inverse compression over the received symbol, we can obtain the received complex symbol $\tilde{y}_{l,\kappa}$, expressed as

$$\tilde{y}_{l,\kappa} = \frac{1}{\sqrt{K}}\sum_{k=1}^{K} y_{l,k}\omega(\kappa,k). \tag{6}$$

Because the Walsh transform requires only real addition operations, the extra computational complexity added to the system is minimal. On the other hand, according to the column rate returned by the Walsh function, the Walsh transform can decompose the signal into orthogonal rectangular waves, thus avoiding the cumulative effect of quantization errors [31]. The column rate is a generalized frequency determined by the number of zero crossings per unit time spacing [30]. Therefore, the Walsh transform-based symbol compression method is noise-resistant and error-tolerant and can effectively avoid the quantization error. Note that the Walsh transform-based compression method requires that the transmitted symbol number $K$ be a power of two. The reason is that the Walsh transform is an orthogonal transformation of binary sequences. However, this usually has no impact on the transmission performance of the system, since we can solve this problem by supplementing it with zeros [31].

### 3.2. Discrete-time model

At time $t \in [-OT_0/2\ , OT_0/2\ + (K-1)T)$, we sample the base pulse with rate $f_s = 1/\Delta t$. Then, the discrete time expression for the transmitted signal $s(n)$ can be written as

$$s(n) = \sqrt{\Delta t}\sum_{k=1}^{K}\sum_{l=1}^{L} x_{l,k}g_{l,k}((n-1)\Delta t - \frac{OT_0}{2}). \tag{7}$$

Where $O$ denotes the overlapping factor, $T_0$ denotes the time scale, which depends on the time spacing, $\Delta t$ denotes the sampling spacing, $n = 1,\dots,N$ with $N = (OT_0+T(K-1))f_s$ denotes the number of samples.

To simplify the representation, we denote the sampled values of the base pulse by the vector $\mathbf{g}_{l,k} \in \mathbb{C}^{N\times 1}$. Then, the sample vectors are integrated into a transmission matrix $\mathbf{G} = [\mathbf{g}_{1,1},\dots\mathbf{g}_{L,K}] \in \mathbb{C}^{N\times LK}$. We denote all transmitted complex data symbols by $\tilde{\mathbf{x}} = [x_{1,1},\dots x_{L,K/2}\,]^T \in \mathbb{C}^{LK/2\times 1}$ and the corresponding compression matrix by $\mathcal{W} \in \mathbb{R}^{LK\times LK/2}$. Then, the received complex symbols $\tilde{\mathbf{y}} = [y_{1,1},\dots y_{L,K/2}\,]^T \in \mathbb{C}^{LK/2\times 1}$ can be expressed as

$$\begin{aligned} &\tilde{\mathbf{y}} = \mathcal{W}^H\mathbf{G}^H\mathbf{H}\mathbf{G}\mathcal{W}\tilde{\mathbf{x}} + \mathbf{n} \\ &st.\quad \mathcal{W}^H\mathbf{G}^H\mathbf{G}\mathcal{W} = \mathbf{I}_{LK/2}\,. \end{aligned} \tag{8}$$

Where $\mathbf{H} \in \mathbb{C}^{N\times N}$ denotes the Time-variant convolution matrix of the channel and $\mathbf{n} \sim \mathcal{CN}(\mathbf{0}, P_n\mathcal{W}^H\mathbf{G}^H\mathbf{G}\mathcal{W})$ the Gaussian noise with power $P_n$. According to Eqs. (5) and (6), we can only obtain the compression matrix at the subcarrier position $l$. However, the compression matrix is the same for different subcarrier positions. Thus, we can map the compression matrix of one subcarrier position to all subcarrier positions. Thereby, the global compression matrix in Eq. (8) is obtained. To further reduce the computational complexity, we consider obtaining the compression matrix by utilizing the fast Walsh transform with the divide-and-conquer method. The detailed steps are given by **Alg. 1**.

**Algorithm 1:** Compression matrix generation based on the fast Walsh transform.

**Input:** Symbol number $K$, Subcarrier number $L$.
**Output:** Compression matrix $\mathcal{W} \in \mathbb{R}^{LK\times LK/2}$.
Step 1: Initialize $\mathcal{W} = \varnothing$, Subcarrier index vector $\boldsymbol{\vartheta} = [1,\cdots,L]^T \otimes \mathbf{1}^{1\times K}$, Column index $\boldsymbol{\vartheta}_c = [\boldsymbol{\vartheta}]_{:,2\kappa-1}$, $\kappa = 1,\cdots,K/2$.
Step 2: Obtain the Walsh matrix, $\boldsymbol{\omega} = \sqrt{K}\mathscr{F}(\mathbf{I}_K,\ K,\ sequency)$.
Step 3: Correctly map the Walsh matrix.
  **for** $i = 1,\cdots,\max(\max(\boldsymbol{\vartheta}))$ **do**
    **if** $\mathrm{mod}(i+\kappa,2) = 0$ **then**
      $[\mathcal{W}]_{\boldsymbol{\vartheta}=i,\boldsymbol{\vartheta}_c=i} = [\boldsymbol{\omega}]_{:,2\kappa-1}$, $\kappa = 1,\cdots,K/2$.
    **else**
      $[\mathcal{W}]_{\boldsymbol{\vartheta}=i,\boldsymbol{\vartheta}_c=i} = [\boldsymbol{\omega}]_{:,2\kappa}$, $\kappa = 1,\cdots,K/2$.
    **end**
  **end**
Step 4: **return** $\mathcal{W} \in \mathbb{R}^{LK\times LK/2}$.

In **Algorithm 1**, $\mathscr{F}(\mathbf{I}_K,\ K,\ sequency)$ denotes the $K$-order Walsh transform for $\mathbf{I}_K$. The coefficients are listed in increasing order, where each row has an additional zero crossing. The algorithm has a time complexity of $\mathcal{O}(K\log K)$ and is easy to implement. Fig. 2 shows the global transmission structure of the described bi-orthogonal FBMC system. Note that channel estimation requires determining the position of the pilot symbols in the symbol alphabet when mapping the data. Therefore, the received symbols need to be inverse compressed before completing the optimal detection (i.e., the equalization operation).

The orthogonal expression of Eq. (4) can be expressed in matrix form as $\mathbf{G}^H\mathbf{G} = \mathbf{I}_{LK}$. In FBMC, orthogonality is denoted as $\Re\{\mathbf{G}^H\mathbf{G}\} = \mathbf{I}_{LK}$. However, we achieve the biorthogonality of FBMC by orthogonal compressed transmission, i.e., $\mathcal{W}^H\mathbf{G}^H\mathbf{G}\mathcal{W} = \mathbf{I}_{LK/2}$. Note that, according to the relevant conclusions of information theory, if the same number of complex symbols are transmitted, then OFDM (without CP), conventional FBMC, and bi-orthogonal FBMC have the same transmission rate. The bi-orthogonal FBMC has the symbol density of $TF = 1$. The reason is that the underlying structure is still conventional FBMC (i.e., OQAM-FBMC).

### 3.3. Interference analysis

The bi-orthogonal FBMC is also subject to the Balian-Low theorem. It satisfies bi-orthogonality, maximum spectral efficiency, and

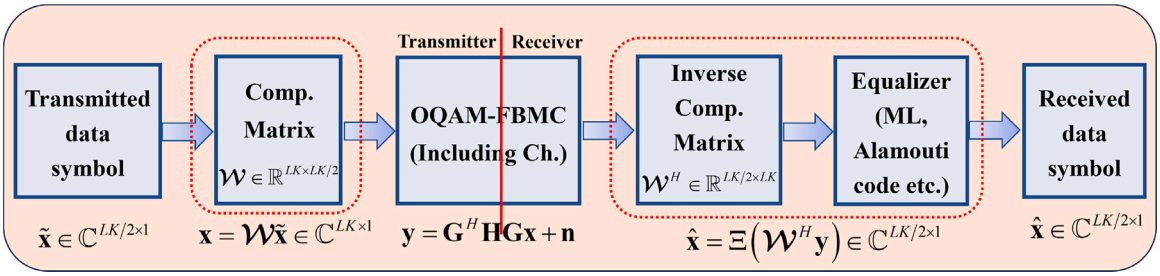


**Fig. 2.** Global transmission structure of the bi-orthogonal FBMC system, in which $\Xi(\cdot)$ denotes the equalization operation. The structure corresponds to Eq. (8) but includes the equalization process. Compared to the conventional FBMC, the bi-orthogonal FBMC deals with data that are all complex.

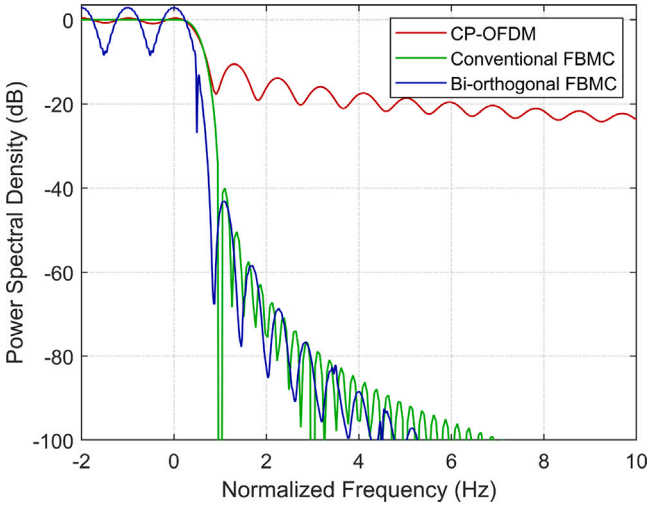


**Fig. 3.** The superior out-of-band attenuation performance of the conventional FBMC is preserved in the bi-orthogonal FBMC. Note that the normalized frequency of the horizontal axis is calculated as $f/F$.

frequency localization simultaneously. However, the time localization becomes suboptimal, which leads to another form of interference. Such interference is different from the inherent imaginary interference of the conventional FBMC. Therefore, we can mitigate it with a simple scheme, see Fig. 4.

To characterize the impact of introducing Walsh transforms into the system, we perform theoretical analysis of the transmit power and power spectral density based on Eqs. (7) and (8). Note that the expected power of the transmitted symbols can be calculated from the transmission matrix [32]. Upon introducing the compression matrix, the transmit power can be computed as

$$\mathbf{P} = \mathrm{diag}\left(\mathbf{G}\mathcal{W}\mathcal{W}^H\mathbf{G}^H\right) \tag{9}$$

Additionally, the power spectral density can be calculated as

$$\begin{aligned} &\mathbf{PSD} = \mathrm{diag}\left\{\mathbf{P}_f\right\} \\ &st.\ \mathbf{P}_f = FFT\left\{\mathbf{G}\mathcal{W}\mathcal{W}^H\mathbf{G}^H\right\} \end{aligned} \tag{10}$$

Where $FFT\{\cdot\}$ denotes the Fast Fourier Transform operation. Fig. 3 shows that the superior spectral properties of the system are preserved.

When the system is configured with PHYDYAS prototype filter and the time localization becomes suboptimal, the pulse exhibits roll-off properties at the boundary. Therefore, at the beginning or end of the data frame, the pulse exhibits outward extension (i.e., transition region). Although the system can transmit each data frame in a bi-orthogonal manner, adjacent data frames can interfere within the transition region when transmitting multiple data frames. This is precisely caused by the deterioration of time localization. If interference power exceeds noise power, then the system performance will be adversely affected.

We consider transmitting $\mathcal{I}$ data frames and assume that the transmission matrix of the $i$th data frame is $\mathbf{G}_i$. Note that these transmission matrices are almost identical, just time-shifted $KT$ from each other. Over a flat fading channel, the biorthogonality of the system is not destroyed. Generally, a flat channel has a complex constant gain (i.e., $\mathbf{H} = \hbar\mathbf{I}_N$). However, the channel coefficient $\hbar$ can be estimated using the pilot structure of Long-Term Evolution (LTE) and it remains constant, which does not affect our interference analysis. Hence, we initially model the flat channel as the identity matrix, i.e., $\mathbf{H} = \mathbf{I}_N$. Interferences come mainly from adjacent data frames. If we do not consider the effect of noise, then the received data symbol $\tilde{\mathbf{y}}_i \in \mathbb{C}^{LK/2\times 1}$ of the $i$th data frame can be expressed as

$$\tilde{\mathbf{y}}_i = \mathcal{W}^H\mathbf{G}_i^H[\mathbf{G}_1, \ldots \mathbf{G}_{\mathcal{I}}]\begin{bmatrix}\mathcal{W}\tilde{\mathbf{x}}_1 \\ \vdots \\ \mathcal{W}\tilde{\mathbf{x}}_{\mathcal{I}}\end{bmatrix}. \tag{11}$$

Where $\tilde{\mathbf{x}}_i$ denotes the transmitted symbol of the $i$th data frame. Thereby, the SIR of the $i$th data frame can be calculated as

$$\begin{aligned} &\mathrm{SIR}_i = \frac{LK}{2\sum_{\alpha=1}^{LK/2}\sum_{\beta=1}^{LK/2}\left|[\mathcal{W}^H\mathbf{G}_i^H\mathbf{G}_j\mathcal{W}]_{\alpha,\beta}\right|^2} \\ &st. \quad \forall i \neq j, \quad i, j = 1, \ldots, \mathcal{I}. \end{aligned} \tag{12}$$

Note that the duration of each frame is $KT$, while the transmission matrices of different frames are time-shifted $KT$ from each other. Frame interference exists when the inner product of the transmission matrices for different frames is not zero. And interferences occur only at the end position of the current frame and the start position of the next frame (i.e., the boundary region). Therefore, we can calculate the specific value of interference based on Eq. (12). The interference can be mitigated if transition time is reserved for each data frame, see Fig. 4, and we call this transition time the guard slot. However, adding guard slots reduces the spectral efficiency, thus we need to weigh the number of guard slots. Based on the above analysis, we can draw the following conclusions for enhancing the SIR:

1. When subcarrier number $L$ is fixed, the larger the transfer length (i.e., symbol numbers $K$) per frame, the larger the SIR.
2. Sacrificing spectral efficiency, we can add guard slots to mitigate interferences and thus improve SIR.

Fig. 5 shows the SIR gain obtained by adding the guard slots. The corresponding spectral efficiency loss rates are shown in Fig. 6. In practice, the number of symbols in one frame is much smaller. For example, the number of symbols for LTE is 14 [33]. However, the purpose of discussing a larger number of symbols is to allow flexibility in adjusting the symbol number. As described in Section 3.1, bi-orthogonal FBMC may require a zero-complement operation on the data symbols. Conventional FBMC can guarantee good transmission

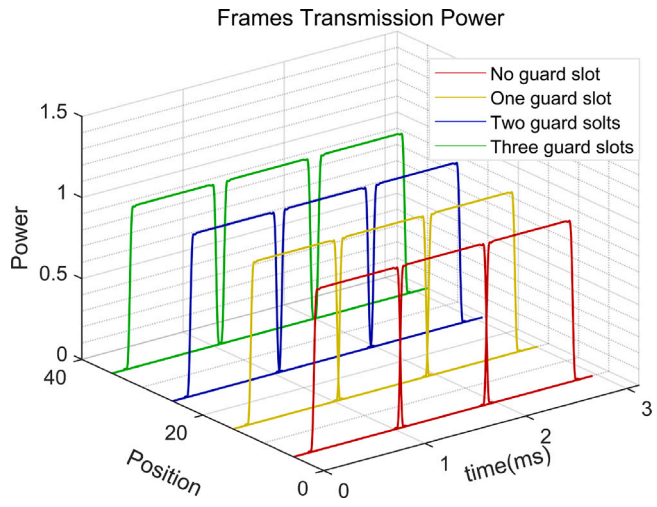


**Fig. 4.** Due to the edge effect, adjacent data frames interfere. Adding guard slots between transmitted frames, we can mitigate the interference and thus enhance the SIR. Note that "Position" is a parameter we introduced just to visualize the power with no concrete meaning.

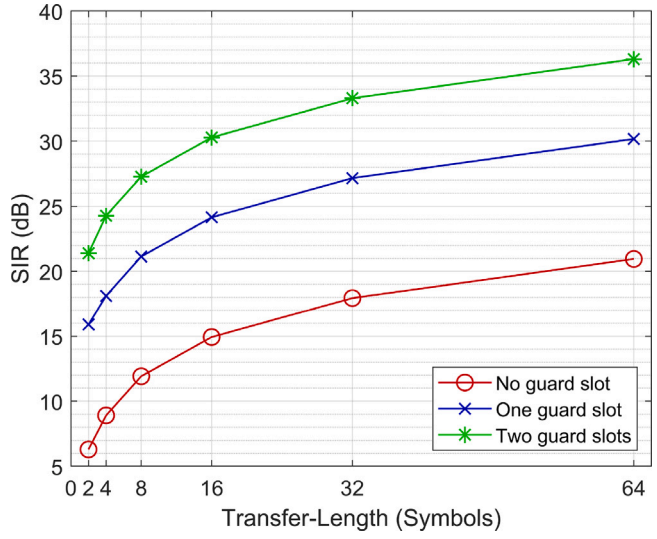


**Fig. 5.** Variation curves of SIR with transfer length over a flat channel. Adding a guard slot, we obtain an SIR gain of about 10 dB. When adding the two guard slots, we obtained an SIR gain of about 15 dB. Note that there are sacrifices to spectral efficiency.

performance without CP [32]. However, the bi-orthogonal FBMC is restricted by the Balian-Low theorem, leading to frame interference. While we add guard slots to mitigate interference, the time resources for transmitting useful signals become occupied. Thereby, the system loses spectral efficiency. However, from Fig. 5, we observe that the loss rate of bi-orthogonal FBMC can still be lower than that of LTE. This indicates that we have retained the spectral efficiency of traditional FBMC to some extent.

Bi-orthogonal FBMC can ignore interference as long as the SNR is much smaller than the SIR when performing multi-frame transmission. The reason is that noise dominates compared to interference. The inter-frame interference occurs only in the boundary region, so we add a guard slot to mitigate the interference. This operation weighs the SIR gain against the spectral efficiency loss rate. If the channel environment is doubly selective fading, then the biorthogonality is destroyed and the SIR deteriorates dramatically.

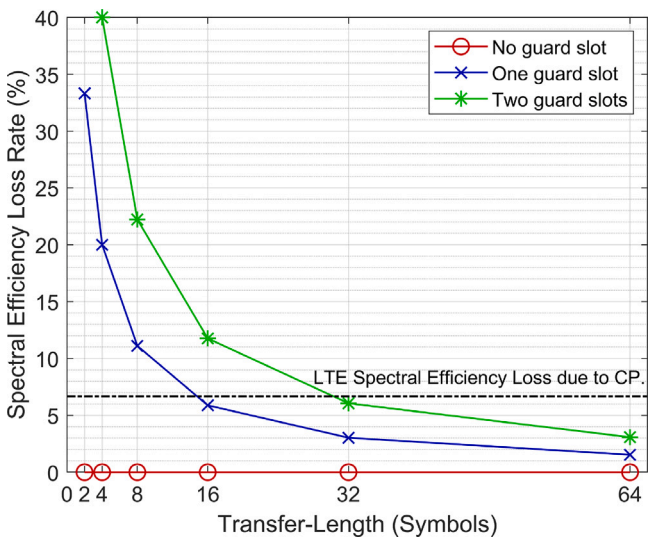


**Fig. 6.** Curves of spectral efficiency loss rate with transfer length. For longer transfer lengths, the efficiency loss rate is close to zero. However, this is difficult to apply to doubly selective channels because the SIR deteriorates dramatically.

Disregarding noise, we introduce a time-varying channel $\mathbf{H} \in \mathbb{C}^{N\times N}$ with multipath fading in Eq. (11). Then, the received data symbol $\tilde{y}_{l,\kappa,i}$ in the $i$th frame can be expressed as

$$\tilde{\mathbf{y}}_{l,\kappa,i} = \left( \begin{bmatrix} \mathcal{W}\tilde{\mathbf{x}}_1 \\ \vdots \\ \mathcal{W}\tilde{\mathbf{x}}_I \end{bmatrix}^T [\mathbf{G}_1, \ldots, \mathbf{G}_I]^T \otimes \mathbf{w}_{l,\kappa}^H \mathbf{G}_i^H \right) \mathrm{vec}\{\mathbf{H}\}. \tag{13}$$

Where $\mathbf{w}_{l,\kappa} \in \mathbb{R}^{LK\times 1}$ denotes the $l + L(\kappa - 1)$-th column vector of $\mathcal{W}$. According to Eq. (13), we can calculate the signal and interference joint power $P_{S_{l,\kappa,i}+I_{l,\kappa,i}} = \mathrm{E}\{|\tilde{y}_{l,\kappa,i}|^2\}$ as

$$\begin{aligned} P_{S_{l,\kappa,i}+I_{l,\kappa,i}} &= \sum_{\mathbb{N}+} \mathrm{diag}\left\{ \mathcal{Q}_{S_{l,\kappa,i}+I_{l,\kappa,i}} \mathbf{R}_H \mathcal{Q}_{S_{l,\kappa,i}+I_{l,\kappa,i}}^H \right\} \\ st.\ \mathcal{Q}_{S_{l,\kappa,i}+I_{l,\kappa,i}} &= [\mathbf{G}_1\mathcal{W}, \ldots, \mathbf{G}_I\mathcal{W}]^T \otimes \mathbf{w}_{l,\kappa}^H \mathbf{G}_i^H. \end{aligned} \tag{14}$$

Where $\mathbf{R}_H = \mathrm{E}\{\mathrm{vec}\{\mathbf{H}\}\mathrm{vec}\{\mathbf{H}\}^H\}$ denotes the channel correlation matrix. Similarly, the signal power $P_{S_{l,\kappa,i}}$ is

$$\begin{aligned} P_{S_{l,\kappa,i}} &= \mathcal{Q}_{S_{l,\kappa,i}} \mathbf{R}_H \mathcal{Q}_{S_{l,\kappa,i}}^H \\ st.\ \mathcal{Q}_{S_{l,\kappa,i}} &= \mathbf{w}_{l,\kappa}^T \mathbf{G}_i^T \otimes \mathbf{w}_{l,\kappa}^H \mathbf{G}_i^H. \end{aligned} \tag{15}$$

According to Eqs. (14)–(15), the average SIR of the $i$th data frame is

$$\mathrm{SIR}_i = \frac{\sum_{l=1}^{L}\sum_{\kappa=1}^{K/2} P_{S_{l,\kappa,i}}}{\sum_{l=1}^{L}\sum_{\kappa=1}^{K/2} (P_{S_{l,\kappa,i}+I_{l,\kappa,i}} - P_{S_{l,\kappa,i}})}. \tag{16}$$

Over a doubly selective channel, the advantage of longer transfer lengths to obtain higher SIR is diminished. The reason is that the orthogonality of a single data frame is destroyed, besides the interference between data frames. The longer the transfer length, the harder the orthogonality is to maintain. Therefore, the transfer length should not be too long for doubly selective channel transmissions. We suggest scaling down the symbol number of a single data frame, and then, ensuring the system throughput by increasing the number of transmitted frames.

## 4. MIMO transmission

In conventional FBMC, imaginary interference seriously affects the performance of ML detection. In particular, the compatibility of MIMO is limited [34]. Many articles combining FBMC and MIMO have left serious flaws. For example, [35] heavily relies on channel information from the transmitter, while [36] has high computational complexity.

Bi-orthogonal FBMC can address the problems caused by imaginary interference and realize compatibility with many techniques in OFDM. This allows the system to obtain the same complexity as MIMO in OFDM.

To mitigate interference between data frames, we add a guarded slot between adjacent data frames. Then, the global compression matrix is expressed as

$$\widehat{\mathcal{W}} = \left[\mathbf{0}_{L,LK/2}, \mathcal{W}\right] \in \mathbb{R}^{L(K+1)\times LK/2}. \tag{17}$$

We consider an $A\times A$ MIMO multiplexing system and transmit different data symbols on different antennas. If the $a$th transmitting antenna transmits $I$ data symbol frames, then the compressed data symbol $\bar{\mathbf{x}}_a \in \mathbb{C}^{L(K+1)\times I}$ can be expressed as

$$\bar{\mathbf{x}}_a = \widehat{\mathcal{W}}\left[\tilde{\mathbf{x}}_{a,1}, \ldots, \tilde{\mathbf{x}}_{a,I}\right]. \tag{18}$$

Where $\tilde{\mathbf{x}}_{a,i} \in \mathbb{C}^{LK/2\times 1}$ denotes the $i$th data frame transmitted by the $a$th transmitting antenna. Thereby, the transmitted signal $\mathbf{s}_a \in \mathbb{C}^{N\times 1}$ of the $a$th transmitting antenna can be expressed as

$$\mathbf{s}_a = \widehat{\mathbf{G}}\mathrm{vec}(\bar{\mathbf{x}}_a). \tag{19}$$

Where $\widehat{\mathbf{G}} = [\mathbf{G}_1, \ldots \mathbf{G}_I] \in \mathbb{C}^{N\times IL(K+1)}$. At the receiver, the received signal from all antennas can be expressed as

$$\begin{bmatrix}\mathbf{r}_1\\ \vdots\\ \mathbf{r}_A\end{bmatrix} = \begin{bmatrix}\mathbf{H}_{1,1} & \cdots & \mathbf{H}_{1,A}\\ \vdots & \ddots & \vdots\\ \mathbf{H}_{A,1} & \cdots & \mathbf{H}_{A,A}\end{bmatrix}\begin{bmatrix}\mathbf{s}_1\\ \vdots\\ \mathbf{s}_A\end{bmatrix} + \begin{bmatrix}\mathbf{n}_1\\ \vdots\\ \mathbf{n}_A\end{bmatrix}. \tag{20}$$

Where $\mathbf{H}_{i,j} \in \mathbb{C}^{N\times N}$ denotes the time-varying convolution matrix from the $i$th antenna to the $j$th antenna, and $\mathbf{n}_i$ the complex Gaussian noise of the $i$th antenna. Then, the symbol $\tilde{\mathbf{y}}_{a,i} \in \mathbb{C}^{LK/2\times 1}$ of the $i$th data frame received by the $a$th receiving antenna can be expressed as

$$\tilde{\mathbf{y}}_{a,i} = \widehat{\mathcal{W}}^H \mathbf{G}_i^H \mathbf{r}_a. \tag{21}$$

Thereby, all the data symbol $\tilde{\mathbf{y}}_a \in \mathbb{C}^{LK/2\times I}$ received by the $a$th receiving antenna is

$$\tilde{\mathbf{y}}_a = \left[\tilde{\mathbf{y}}_{a,1}, \ldots, \tilde{\mathbf{y}}_{a,I}\right]. \tag{22}$$

In practical transmissions, perfect channel information is not available at the receiver. Therefore, we adopt the diamond-shaped pilot structure for channel estimation, similar to Long Term Evolution (LTE). The estimated channel information is then utilized for ML detection.

## 5. Numerical analysis

To verify our scheme, we employ the following parameter configuration: The carrier frequency is 2.5 GHz. The subcarrier number $L = 128$. The subcarrier spacing is 15 KHz. The sampling rate is $f_s = 3.84$ MHz. The overlapping factor is $O = 4$. We adopt the "Vehicular B" channel model of 3GPP 38.900, with a wide-sense stationary uncorrelated scattering path number of 200. Future wireless standards, like 5G or beyond, need to deal with high-mobility scenarios. Therefore, we investigate the SIR scenario at different velocities. Fig. 7 shows the SIR variations with different mobile velocities. At high mobility (i.e., high Doppler shift), the SIR deteriorates dramatically. This can significantly impact the Bit Error Rate (BER) performance. One possible solution is to employ Turbo coding [37]. Note that this paper does not verify channel coding, but rather examines the fundamental performance of bi-orthogonal FBMC.

The above parameter configurations allow the bi-orthogonal FBMC and CP-OFDM to have the same bit rate for fair comparison. However, bi-orthogonal FBMC has better spectral properties and thus is able to use larger subcarrier numbers. We consider that the system transmits a total of three data frames, with each frame having a transfer length of $K = 16$. Then, we insert a guard slot between adjacent data frames. This leads to a transmission time of $(2K + 1)/(2F) = 1.1$ ms per data frame (Note that FBMC based on offset-QAM compresses the time spacing

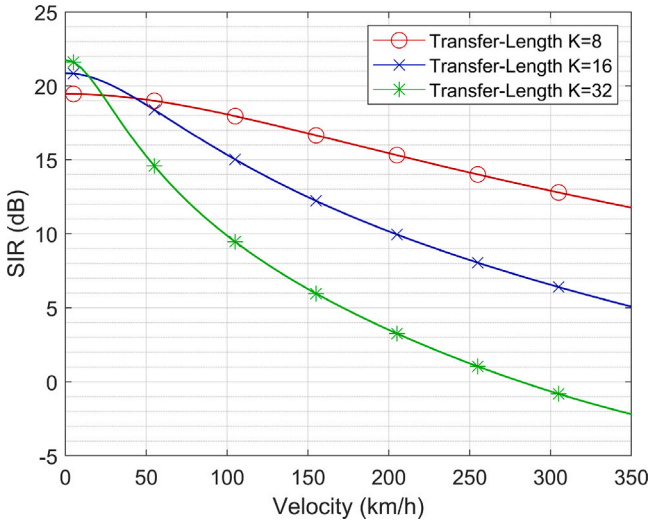


**Fig. 7.** Variation curves of SIR with different mobile velocities. Higher mobile velocities reduce the SIR because orthogonality is destroyed. On the other hand, longer transfer lengths over doubly selective channels also worsen the SIR. However, at a mobile velocity of 0, a longer transfer length again obtains a higher SIR. This also verifies conclusion 1.

to $T = 0.5/F$.). For CP-OFDM, we take the CP time spacing to be $T_{CP} = 2.085$ μs. The transfer length of each frame is also $K = 16$. Therefore, CP-OFDM has a transmission time of $K(1/F + T_{CP}) = 1.1$ ms per data frame.

In this section analysis, we consider a 2 × 2 MIMO multiplexing system that transmits independent bit streams over two antennas. At the receiver, we employ Zero Forcing (ZF) detection and ML detection [20] (Not applicable in conventional FBMC because of imaginary interference.). Also, we consider a 2 × 1 Alamouti space–time block code transmission scheme [22]. For a fair comparison, we assume that OFDM and bi-orthogonal FBMC have the same signal power and the same frequency spacing. When both have the same subcarrier number, they have the same SNR [38], which can be calculated as

$$\mathrm{SNR} = 10\log\left(\frac{f_s}{P_n F L}\right)(\mathrm{dB}). \tag{23}$$

Fig. 8 shows the relation between BER and SNR. Bi-orthogonal FBMC has nearly the same BER performance as OFDM, which verifies the feasibility of our scheme in practical applications. Numerically, the BER of our scheme is improved by about 5% compared to [23]. However, ML detection and Alamouti code nearly fail in conventional FBMC. Note that the ML detection in this paper is conditioned on Gaussian-distributed noise, thus approximating the ML performance. Therefore, ML detection can characterize the actual situation when noise dominates.

If we consider the case in which FBMC is realized as an efficient Fast Fourier Transform (FFT), then the FFT size is $N_{FFT} = f_s/F \geq L$. Note that the system cannot work at the critical sampling rate ($N_{FFT} = L$) in practical applications. The reason is that this leads to high OOB emissions [32]. Since offset-QAM -based FBMC compresses the time spacing, which leads to twice as many computations for bi-orthogonal FBMC as for OFDM (without CP). Thus, the computational complexity of our transmission scheme is approximately twice as high as CP-OFDM, as expressed by

$$\frac{2(N_{FFT}\log N_{FFT} + ON_{FFT})}{N_{FFT}\log N_{FFT}} \approx 2. \tag{24}$$

Where $N_{FFT}\log N_{FFT}$ corresponds to the Inverse Fast Fourier Transform (IFFT) required for FBMC and OFDM. $ON_{FFT}$ corresponds to the prototype filter product required for FBMC. Note that we do not consider the extra computational effort involved in generating the compression matrix.

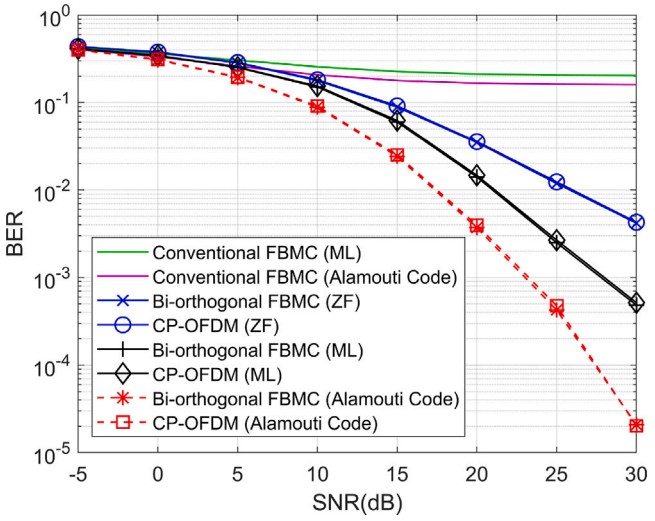


**Fig. 8.** Curves of BER versus SNR. Bi-orthogonal FBMC has nearly the same BER as OFDM. However, with high SNR, the BER performance of ML becomes reduced. The reason is that interference starts to dominate compared to noise.

## 6. Conclusion

The proposed bi-orthogonal FBMC transmission scheme in this paper is compatible with CP-OFDM in many aspects. For example, many MIMO techniques known from OFDM can be directly applied. It retains many outstanding properties of the traditional FBMC. Examples include favorable spectral performance, much lower OOB emissions, and no CP required. Additionally, the MIMO technique works very robustly in FBMC once we recover the biorthogonality of the system. This bi-orthogonal FBMC transmission based on the Walsh transform is applicable to many practical communication scenarios, including uplink transmission for wireless communication and Machine-to-machine (M2M) communication. As described before, we recommend adding one guard slot to improve the SIR when adopting the proposed transmission scheme.

## CRediT authorship contribution statement

**Ying Wang:** Conceptualization, Methodology, Software, Supervision, Validation, Writing – original draft. **Qiang Guo:** Writing – review & editing. **Jianhong Xiang:** Data curation, Project administration. **Linyu Wang:** Writing – review & editing. **Yang Liu:** Funding acquisition.

## Declaration of competing interest

The authors declare that they have no known competing financial interests or personal relationships that could have appeared to influence the work reported in this paper.

## Data availability

Data will be made available on request.

## Acknowledgments

This work is supported in part by Fundamental Research Funds for the Central Universities, China [3072022CF0801], National Key R and D Program, China [2018YFE0206500], and Sichuan Provincial Key Laboratory of Agile Intelligent Computing Project Fund. We thank all the anonymous reviewers who generously contributed their time and efforts.

## Appendix. Proof of biorthogonality

To intuitively illustrate that our proposed system is orthogonal, we prove the constraints of Eq. (8) by a simple example, i.e., the subcarrier number $L = 3$ and the symbol number $K = 2$. Then, $\mathbf{G}^H\mathbf{G} \in^{6\times6}$ can be expressed as

$$\mathbf{G}^H\mathbf{G} = \begin{bmatrix} 1 & 0.2393j & 0 & 0.5644j & 0.2058j & 0 \\ -0.2393j & 1 & 0.2393j & -0.2058j & -0.5644j & -0.2058j \\ 0 & -0.2393j & 1 & 0 & 0.2058j & 0.5644j \\ -0.5644j & 0.2058j & 0 & 1 & 0.2393j & 0 \\ -0.2058j & 0.5644j & -0.2058j & -0.2393j & 1 & 0.2393j \\ 0 & 0.2058j & -0.5644j & 0 & -0.2393j & 1 \end{bmatrix}. \tag{25}$$

The compression matrix $\mathcal{W} \in \mathbb{R}^{6\times3}$ is given by

$$\mathcal{W} = \frac{1}{\sqrt{2}} \begin{bmatrix} 1 & 0 & 0 \\ 0 & 1 & 0 \\ 0 & 0 & 1 \\ -1 & 0 & 0 \\ 0 & 1 & 0 \\ 0 & 0 & -1 \end{bmatrix}. \tag{26}$$

According to Eqs. (25) and (26), we can easily verify that $\mathcal{W}^H\mathbf{G}^H\mathbf{G}\mathcal{W} = \mathbf{I}_3$. In fact, we can determine a compression matrix and satisfy the constraints of Eq. (8) by Algorithm 1 for any $L$ and $K$. However, as mentioned before, the symbol number $K$ must be a power of two. Thus, we require adding zeros to solve this problem.

## References

[1] Màrius Caus, Ana I. Pérez-Neira, FBMC-Based Random Access Signal Design and Detection for LEO Base Stations, IEEE Trans. Wireless Commun. 22 (3) (2022) 2156–2170.
[2] Sumaila Mahama, Yahya J Harbi, David Grace, Alister G Burr, Multi-User Interference Cancellation for Uplink FBMC-Based Multiple Access Channel, IEEE Commun. Lett. 25 (8) (2021) 2733–2737.
[3] K. Vasudevan, Digital Communications and Signal Processing, vol. 81, (no. 7371) Universities Press, India, Hyderabad, 2010, p. 575, ISBN.
[4] Ronald Nissel, Stefan Schwarz, Markus Rupp, Filter bank multicarrier modulation schemes for future mobile communications, IEEE J. Sel. Areas Commun. 35 (8) (2017) 1768–1782.
[5] Kasturi Vasudevan, Coherent detection of turbo-coded OFDM signals transmitted through frequency selective Rayleigh fading channels with receiver diversity and increased throughput, Wirel. Pers. Commun. 82 (3) (2015) 1623–1642.
[6] K. Vasudevan, Near Capacity Signaling over Fading Channels using Coherent Turbo Coded OFDM and Massive MIMO, Int. J. Adv. Telecommun. 10 (1 & 2) (2017).
[7] K Vasudevan, Shivani Singh, A Phani Kumar Reddy, S Mohammady, Coherent receiver for turbo coded single-user massive MIMO-OFDM with retransmissions, in: Multiplexing, IntechOpen, 2019, pp. 1–21.
[8] Iandra Galdino Andrade, Didier Le Ruyet, Marcello LR de Campos, Rostom Zakaria, Bit Error Probability Expressions for QAM-FBMC Systems, IEEE Commun. Lett. 26 (5) (2022) 994–998.
[9] Sumaila Mahama, Yahya J Harbi, Alister G Burr, David Grace, A non-orthogonal waveform design with iterative detection and decoding for narrowband IoT applications, in: 2019 European Conference on Networks and Communications (EuCNC), IEEE, 2019, pp. 315–319.
[10] Davide Mattera, Mario Tanda, Maurice Bellanger, Performance analysis of some timing offset equalizers for FBMC/OQAM systems, Signal Process. 108 (2015) 167–182.
[11] Mario Tanda, Asymptotic performance of FBMC-PAM systems in frequency-selective Rayleigh fading channels, Signal Process. 201 (2022) 108693.
[12] Yuhao Qi, Jian Dang, Zaichen Zhang, Liang Wu, Yongpeng Wu, Efficient Channel Equalization and Performance Analysis for Uplink FBMC/OQAM-Based Massive MIMO Systems, IEEE Trans. Veh. Technol. (2023).
[13] AlaaEddin Loulou, Juha Yli-Kaakinen, Markku Renfors, Advanced low-complexity multicarrier schemes using fast-convolution processing and circular convolution decomposition, IEEE Trans. Signal Process. 67 (9) (2019) 2304–2319.
[14] Davide Mattera, Mario Tanda, Maurice Bellanger, Filter bank multicarrier with PAM modulation for future wireless systems, Signal Process. 120 (2016) 594–606.

[15] Samael Sarmiento, Jose A Altabas, Salvatore Spadaro, Jose A Lazaro, Experimental assessment of 10 Gbps 5G multicarrier waveforms for high-layer split U-DWDM-PON-based fronthaul, J. Lightwave Technol. 37 (10) (2019) 2344–2351.
[16] Jeffrey G Andrews, Stefano Buzzi, Wan Choi, Stephen V Hanly, Angel Lozano, Anthony CK Soong, Jianzhong Charlie Zhang, What will 5G be? IEEE J. Sel. Areas Commun. 32 (6) (2014) 1065–1082.
[17] Gerhard Wunder, Peter Jung, Martin Kasparick, Thorsten Wild, Frank Schaich, Yejian Chen, Stephan Ten Brink, Ivan Gaspar, Nicola Michailow, Andreas Festag, et al., 5GNOW: non-orthogonal, asynchronous waveforms for future mobile applications, IEEE Commun. Mag. 52 (2) (2014) 97–105.
[18] Ahmad Rezazadeh Reyhani, Behrouz Farhang-Boroujeny, An analytical study of circularly pulse-shaped FBMC-OQAM waveforms, IEEE Signal Process. Lett. 24 (10) (2017) 1503–1506.
[19] Rostom Zakaria, Didier Le Ruyet, Analysis of the FFT-FBMC equalization in selective channels, IEEE Signal Process. Lett. 24 (6) (2017) 897–901.
[20] Rostom Zakaria, Didier Le Ruyet, A novel filter-bank multicarrier scheme to mitigate the intrinsic interference: Application to MIMO systems, IEEE Trans. Wireless Commun. 11 (3) (2012) 1112–1123.
[21] Suchun Zhang, Mengjiao Zhang, Shi Jin, Chao-Kai Wen, Low-complexity detection for MIMO C-FBMC using orthogonal approximate message passing, IEEE Signal Process. Lett. 26 (1) (2018) 34–38.
[22] Chrislin Lélé, Pierre Siohan, Rodolphe Legouable, The alamouti scheme with CDMA-OFDM/OQAM, EURASIP J. Adv. Signal Process. 2010 (2010) 1–13.
[23] Ronald Nissel, Markus Rupp, Enabling low-complexity MIMO in FBMC-OQAM, in: 2016 IEEE Globecom Workshops (GC Wkshps), IEEE, 2016, pp. 1–6.
[24] Ying Wang, Qiang Guo, Jianhong Xiang, Yang Liu, Doubly selective channel estimation and equalization based on ICI/ISI mitigation for OQAM-FBMC systems, Phys. Commun. 59 (2023).
[25] Maurice Bellanger, D. Le Ruyet, D. Roviras, M. Terré, J Nossek, L Baltar, Q Bai, D Waldhauser, M Renfors, T Ihalainen, et al., FBMC physical layer: a primer, PHYDYAS 25 (4) (2010) 7–10.
[26] Kasturi Vasudevan, Surendra Kota, Lov Kumar, Himanshu Bhusan Mishra, Turbo Coded OFDM-OQAM Using Hilbert Transform, 2023, arXiv preprint arXiv:2309.09620.
[27] Ronald Nissel, Jiri Blumenstein, Markus Rupp, Block frequency spreading: A method for low-complexity MIMO in FBMC-OQAM, in: 2017 IEEE 18th International Workshop on Signal Processing Advances in Wireless Communications, SPAWC, IEEE, 2017, pp. 1–5.
[28] Hans G. Feichtinger, Thomas Strohmer, Gabor Analysis and Algorithms: Theory and Applications, Springer Science & Business Media, 2012.
[29] K.G. Beauchamp, Walsh Functions and Their Applications, Academic Press, 1975.
[30] Tom Beer, Walsh transforms, Amer. J. Phys. 49 (5) (1981) 466–472.
[31] L.R. Brewster, Applications of Walsh and Related Functions with an Introduction to Sequency Theory, Commun. Radar Signal Process. IEE Proc. F 133 (1) (1986) 127–128.
[32] Ronald Nissel, Markus Rupp, Pruned DFT-spread FBMC: Low PAPR, low latency, high spectral efficiency, IEEE Trans. Commun. 66 (10) (2018) 4811–4825.
[33] Ronald Nissel, Markus Rupp, On pilot-symbol aided channel estimation in FBMC-OQAM, in: 2016 IEEE International Conference on Acoustics, Speech and Signal Processing, ICASSP, IEEE, 2016, pp. 3681–3685.
[34] Ali A Zaidi, Jian Luo, Robin Gerzaguet, Andreas Wolfgang, Richard J Weiler, Jaakko Vihriäla, Tommy Svensson, Yinan Qi, Hardy Halbauer, Zhao Zhao, et al., A preliminary study on waveform candidates for 5G mobile radio communications above 6 GHz, in: 2016 IEEE 83rd Vehicular Technology Conference (VTC Spring), IEEE, 2016, pp. 1–6.
[35] Miquel Payaró, Antonio Pascual-Iserte, Montse Nájar, Performance comparison between FBMC and OFDM in MIMO systems under channel uncertainty, in: 2010 European Wireless Conference, EW, IEEE, 2010, pp. 1023–1030.
[36] Ana I Perez-Neira, Marius Caus, Rostom Zakaria, Didier Le Ruyet, Eleftherios Kofidis, Martin Haardt, Xavier Mestre, Yao Cheng, MIMO signal processing in offset-QAM based filter bank multicarrier systems, IEEE Trans. Signal Process. 64 (21) (2016) 5733–5762.
[37] K. Vasudevan, K. Madhu, Shivani Singh, Data Detection in Single User Massive MIMO Using Re-Transmissions, Open Signal Process. J. 6 (1) (2019).
[38] Ronald Nissel, Sebastian Caban, Markus Rupp, Experimental evaluation of FBMC-OQAM channel estimation based on multiple auxiliary symbols, in: 2016 IEEE Sensor Array and Multichannel Signal Processing Workshop, SAM, IEEE, 2016, pp. 1–5.